The counteracting effect of the friction moment against the tibial rotational moment driven by the ground reaction force in an early stance phase of cutting maneuver among healthy male athletes

Issei Ogasawara, Megumi Nambo, Yuki Uno, Gajanan S. Revankar, Kaho Umegaki, Haotian Cheng, Shoji Konda, Tomoyuki Matsuo, Tatsuo Mae, Ken Hashizume & Ken Nakata

Published online: 28 Oct 2022.

Submit your article to this journal ⬀

Article views: 229

View related articles ⬀

View Crossmark data ⬀

Routledge
Taylor & Francis Group

SPORTS MEDICINE AND BIOMECHANICS

Check for updates

The counteracting effect of the friction moment against the tibial rotational moment driven by the ground reaction force in an early stance phase of cutting maneuver among healthy male athletes

Issei Ogasawara [a,b], Megumi Nambo[a], Yuki Uno [a], Gajanan S. Revankar [a,c], Kaho Umegaki[a], Haotian Cheng[a], Shoji Konda [a,b], Tomoyuki Matsuo [a], Tatsuo Mae[b], Ken Hashizume[a] and Ken Nakata[a]

[a]Department of Health and Sports Sciences, Graduate School of Medicine, Osaka University, 1-17 Machikaneyama-cho 560-0043, Toyonaka, Osaka, Japan; [b]Department of Sports Medical Biomechanics, Graduate School of Medicine, Osaka University, 2-2 Yamada-oka 565-0871, Suita, Osaka, Japan; [c]Department of Neurology, Graduate School of Medicine, Osaka University

ABSTRACT

The ground reaction force (GRF) is known to produce tibial internal rotation loading associated with the stress in the anterior cruciate ligament (ACL). However, it is unclear whether the friction moment (FM; the moment due to horizontal shoe-floor friction, acting around the vertical axis at the GRF acting point) facilitates or restrains the effect of GRF-driven tibial rotation loading during cutting. The 45° cutting motions with forefoot/rearfoot strikes were captured simultaneously with GRF and FM data from 23 healthy males. The FM- and GRF-driven tibial rotation moments were calculated. Time-series correlation between FM- and GRF-driven tibial rotation moments and the orientation relationship among those moment vectors was investigated. The FM-driven tibial rotation moment negatively correlated with the GRF-driven one within the first 10% of stance phase. The peak regression slope value was −0.34 [SD 0.33] for forefoot and −1.64 [SD 1.76] for rearfoot strikes, showing significant difference from zero (SPM one-sample t-test, $p < 0.05$). The FM-driven tibial "external" rotation moment counteracted the GRF-driven tibial "internal" rotation moment within first 10% of the stance phase in most trials, suggesting that the FM-driven tibial rotation moment potentially diminishes the effect of GRF-driven one and may reduce ACL injury risk during cutting.

Introduction

Anterior cruciate ligament (ACL) serves as a restraint for tibial anterior force (Sakane et al., 2004), and combined knee valgus and tibial internal rotation loadings (Markolf et al., 1995; Oh et al., 2012; Shin et al., 2011). ACL also provides proprioceptive feedbacks regarding its kinaesthetic status to the central nervous system (Biedert & Zwick, 1998; Friemert et al., 2005) and thus contributes to the dynamic neuromuscular stability of the knee (Solomonow et al., 1987). Unfortunately, ACL is frequently involved in injuries related to sporting motions such as landing, cutting and stoppings (Boden et al., 2000; Griffin et al., 2000; Ireland, 1999; Krosshaug et al., 2007). Female athletes have two to four times higher ACL injury risk than male counterparts (Arendt & Dick, 1995; Prodromos et al., 2007). Regardless, it is a common concern for both genders (Agel et al., 2016; Mountcastle et al., 2007; Røtterud et al., 2011). Active athletes suffering from ACL injury resulting in knee joint instability are often advised to have surgical reconstruction and a prolonged rehabilitation in order to return to sports (Grevnerts et al., 2021). However, not all ACL-reconstructed athletes satisfactorily regain their competitive performance when they make a return to sports (Ardern et al., 2014). In addition, prolonged ACL insufficiency results in an early onset of osteoarthritis deteriorating the athlete's quality of life (Lohmander et al.,

2004; Porat et al., 2004). It is therefore pertinent that the mitigation of ACL injury risk in sports is crucial for athletes.

In sports, up to 70% of ACL rupture typically occurs in the early deceleration phase of cutting or single-leg landing in a non-contact manner, without a direct blow to the knee from other players (Boden et al., 2000; Griffin et al., 2000; Ireland, 1999; Krosshaug et al., 2007). Videography of actual ACL injury has estimated that the time frame from initial foot contact (IC) to the ACL disruption is about 40 ms (Koga et al., 2011). Such feature of ACL injury in sports indicated that a large ground reaction force (GRF) acting at the stance foot results in an out-of-plane knee valgus (Kristianslund et al., 2014; McLean et al., 2005; Sigward & Powers, 2007) and/or tibial internal rotation moment (Quatman et al., 2010; Shimokochi & Shultz, 2008) as well as a high tibiofemoral compression force (Meyer et al., 2008; Meyer & Haut, 2005, 2008) which is sufficient to rupture the ACL. Specifically, the internal tibial rotation moment is considered as a significant contributor to increase the stress to the ACL (Markolf et al., 1995; Oh et al., 2012; Oh et al., 2012). A cadaver study reported that the tibial internal rotation moment combined with the anterior tibial force produced about a 2-fold ACL force than the tibial external rotation moment combined with anterior tibial force (Markolf et al., 1995). A similar finding was replicated in a more sports-relevant pivot landing experiment using human knee

specimens as well as a computational knee model (Oh et al., 2012). A recent lab-controlled study reported that the tibial internal rotation moment due to GRF more frequently co-occurred with the knee valgus moment during rearfoot strikes than forefoot strikes (Ogasawara et al., 2020). The high incidence of non-contact ACL injury with heel strike has been reported in wide range of sports (Boden et al., 2000; Montgomery et al., 2016). Collectively, these studies suggest that the management of internal tibial rotation loading caused by GRF during foot impact is a key strategy to mitigate the subsequent risky knee loading status.

In a non-contact situation, one possible mechanism that controls the GRF-driven tibial internal rotation moment is the friction moment (FM, so called free moment). The FM is a moment vector acting around the vertical axis at the centre of pressure (CoP) of the stance foot, which is produced by the horizontal friction force acting within the base of support (BoS). Since the FM acting at CoP transfers to knee joint through tibia (Wannop et al., 2010), the GRF and FM, both acting at the CoP, mechanically interact with each other at knee and alter the resultant knee moment. Robinson et al. (2017) have reported that the positive peak of FM (anatomical direction was unknown) within weight acceptance phase of sidestepping had significant correlations with the multi-axis knee moments of mid-stance phase. David et al. (2021) investigated the effect of FM on the ACL injury risk-relevant knee loadings in 90° cutting tasks and suggested that the internally-directed FM acting at CoP may functionally increase the load on ACL. Collectively, these studies suggested in their discussion that the FM may be associated with the potential risk of ACL injury as the discrete FM peaks have been shown to be correlated with the 3D knee moment magnitudes in mid-stance phase of cutting. However, since the FM and the 3D knee moments are expressed in different coordinate systems in these studies, the mechanical effects of the transferred FM on the GRF-driven tibial rotation moment at the knee joint are not fully understood. In addition, it is unclear whether the FM magnitude evolves to be large enough to increase the stress in the ACL within time frame where the ACL injury reported to occur (e.g., less than 40 ms after initial foot contact (Koga et al., 2011)) .

When we focus on an early phase of foot contact when the ACL injury reportedly occurs, the FM-driven tibial rotation moment may potentially diminish the effect of GRF-driven tibial rotation moment if these moments were directed antagonistically. Since both FM- and GRF-driven tibial rotation moments rotate the tibia either internally or externally, there are four combinations of orientation couplings (i.e., internal/internal, internal/external, external/internal, and external/external). Which coupling patterns are stochastically more likely to occur at an early stance phase of cutting has not been studied yet. While the shank is being accelerated towards internal direction by GRF-driven moment around the shank axis, the shoe-floor friction force which resists the GRF-driven shoe-floor movement at CoP would be expected to produce the opposing reaction moment around the shank axis as well. If this assumption were to be true, utilization of FM would turn out to be a practical strategy to reduce the risk of tibial internal rotation driven by GRF especially at an early deceleration phase of cutting manoeuvres which is relevant to ACL injury risk.

Therefore, the purpose of this study was to examine whether the FM applied at CoP of the stance limb can counter-act the tibial internal rotation moment caused by the GRF in cutting. Given the context of non-contact ACL injury mechanism, our primary interest was the early stance phase of cutting (e.g., first 40 ms after initial foot contact). However, for the purpose of highlighting the specific features immediately after foot contact and contrasting them with the features after the midstance phase, the data will be reported for the entire stance phase of cutting. The effect of the different foot-strike patterns (forefoot and rearfoot strike) on the interaction between the FM- and GRF-driven tibial rotation moment were also examined. We hypothesized that the tibial rotation moment due to GRF and due to FM are negatively correlated and the actions of those moments oppose each other at an early stance phase of cutting for both foot-strike patterns.

Methods

Ethical

This study was approved by the ethics committee of the Osaka University Hospital ethics board [18082] and the experimenters obtained informed consent from all participants before participation.

Participants

Twenty-three healthy male recreational athletes of the collegiate team sports (basketball, handball, and lacrosse) were recruited. These team sports were selected since they involve the change of direction movement as a basic skill. Inclusion criteria were the athletes who have performed sports for more than three years and at least four practice days per week. Potential participants who had 1) histories of severe lower limb musculoskeletal injuries such as ACL injury or 2) recent histories of the light to moderate lower limb injuries such as ankle sprain within 3 months before the experimental day, and 3) any symptoms or anxieties which prevent performing motion task (45° cutting) were excluded.

Experimental procedure

Participants wore black compression shirts, shorts, and the same type of shoes (THH544-001, ASICS, Japan). Twenty-seven reflective markers were attached onto the bony landmarks detailed in Figure 1A. The motion task investigated was the 45° cutting on the forceplate with the forefoot and rearfoot first foot-strike conditions. The participants were asked to run straight with a speed range of 2.5–3.5 m/s and change their running direction with the single-step on the floor-fixed force-plate towards the opposite direction of the landing limb with the angle of 45° relative to the approach line. The approach speed (the average speed from −0.6 to −0.2 m prior to the forceplate) was measured online with a photo-cell gate (WT24-2B410, SICK, Germany) and provided feedback to the participant for each trial. The cutting angle was shown by a line on the floor (Figure 1B). For the forefoot strike condition, the participants were requested to touch only with their forefoot (around
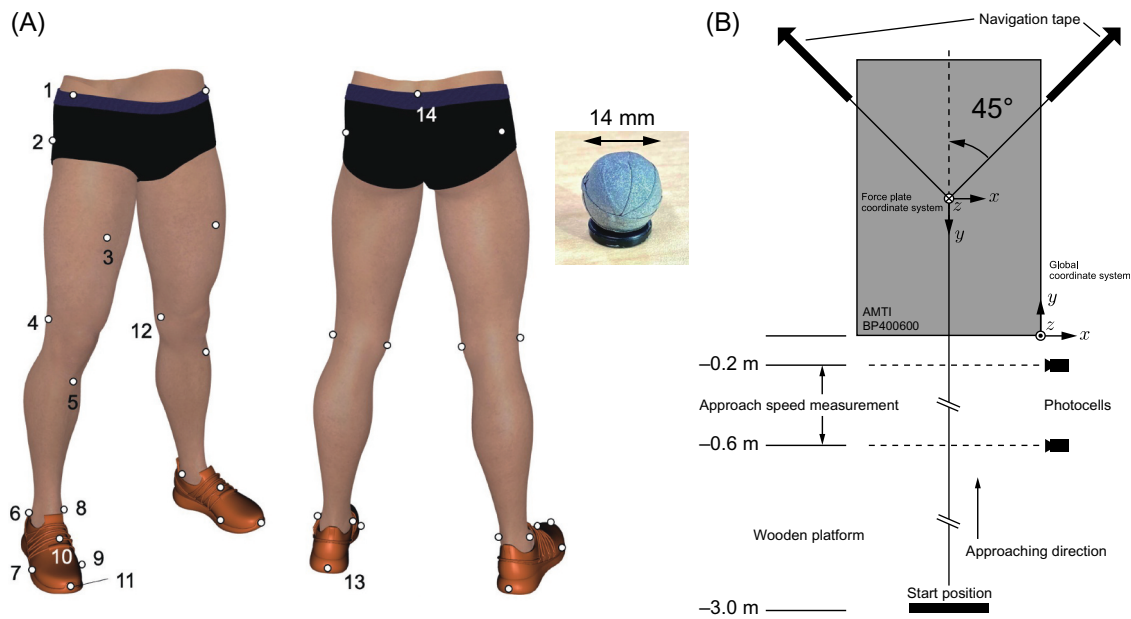
(A)

(B)

Figure 1. Reflective marker position and top view of the experimental environment. The reflective markers (diameter=14 mm) were placed on the body landmarks to construct the kinematic model (A). The marker positions were 1:Anterior superior iliac spine, 2:Greater trochanter, 3:Anterior aspect of mid of thigh, 4: Lateral femoral epicondyle, 5:Tibial tuberosity, 6:Lateral malleolus, 7:Lateral aspect of fifth metatarsophalangeal joint, 8:Medial malleolus, 9:Medial aspect of fifth metatarsophalangeal joint, 10:Proximal edge of first metatarsal bone, 11:Tip of shoe toe, 12:Medial femoral epicondyle, 13: Tip of shoe heel, and 14: Mid-point of both posterior superior iliac spine. The markers 9–13 were put over the sports shoes. The navigation angle (45°) was instructed with the floor tape (B). The global coordinate system (GCS) was defined as a right-hand coordinate system fixed at the corner of the force plate. Seen from the top, the x-axis was the direction pointing towards the right of the participant's approach. The y-axis was along to the participant's approaching direction. The z-axis was the direction perpendicular to x- and y-axis, pointing upwards. The force plate coordinate system was defined as a right-hand coordinate system fixed at the centre of force plate. The x-axis was along with the x-axis of GCS. The y-axis was opposite to the y-axis of GCS. The z-axis was the direction perpendicular to x- and y-axis, pointing downwards (B).

the ball of foot) on the forceplate throughout the stance phase. In contrast, the rearfoot strike condition required the participants hit their heel first on the forceplate and then roll up their weight onto the forefoot region to push-off. The reason for having two different foot-strike conditions was not to compare the statistical differences between two foot-strike conditions but to reproduce the actual sports environment with variations in the foot-strike pattern.

Before data collection, the participants executed a standardized warm-up consisting of stretching and stepping exercise instructed by an experimenter (Y.U.). The participants then practiced the cutting task to familiarize the forefoot/rearfoot strike patterns, change of direction angle (45°), and the approach speed (2.5–3.5 m/s). While practicing, the two experimenters assessed the quality of cutting trials, and the online approach speed monitoring was also performed. At least ten times of practice trials for each leg were performed, but if necessary, the participants were allowed to have more practice trials. In the data collection process, the order of the testing leg (right/left) and foot-strike patterns (forefoot/rearfoot) were randomly determined for each participant. To reduce the effect of the fatigue, we set about 30 seconds of interval between each trial and 3 minutes of rest when the testing leg switching. Taking additional rests was allowed, if necessary, but none of the participants requested those. Two experimenters (N.M. and Y.U.) visually monitored the cutting task requirements, including the correct foot-strike pattern (forefoot/rearfoot), the correct foot placement inside the force-plate, and the appropriate approach speed inside of the targeted

range. If the consensus among the two experimenters was not achieved, the trial was discarded as a failure. The data collection continued until 10 successful trials for each foot-strike pattern with right/left legs were recorded (total 920 trials).

Data measurement

The position data of the reflective markers were captured with the 14 OptiTrack Prime 17 W cameras (sampling rate = 360 Hz, NaturalPoint, Inc., US). The GRF data were collected with the forceplate (BP600400, Ampliter:Gen5, sampling rate = 1,800 Hz, AMTI, US). The recording onset of those equipment were time-synchronized with the clock device (eSync2, NaturalPoint, Inc., US.).

Data processing

The stance phase was defined as the duration where the vertical GRF exceeded 10 N. Both marker and forceplate data were time-normalized for the stance phase, 0% initial contact and 100% end of contact (toe off). Marker data were smoothed with a 2nd order Butterworth-type digital filter (low-pass, zero-time shift). The cut-off frequency for each marker was determined separately by the residual analysis (Winter, 2005) within the range of 12–15 Hz. The forceplate data were smoothed with a 2nd order Butterworth-type digital filter (low-pass, zero-time shift, cut-off frequency: 70 Hz). The (reaction) FM vector $\boldsymbol{\tau}_{\text{frc}} = [0, 0, \tau_{\text{frc}}]^T$ acting around

the participant's CoP from the ground expressed in the force-plate coordinate system (FCS) was calculated as

$$\boldsymbol{\tau}_{\text{frc}} = -(\boldsymbol{\tau}_z - \boldsymbol{r}_{\text{CoP}} \times \boldsymbol{f}_h), \tag{1}$$

where $\boldsymbol{\tau}_z = [0, 0, \tau_z]^T$ was the moment acting around the vertical z-axis of forceplate, $\boldsymbol{r}_{\text{CoP}} = [r_{\text{CoP}_x}, r_{\text{CoP}_y}, 0]^T$ was x- and y-component of CoP position vector going from the force-plate's origin, and $\boldsymbol{f}_h = [f_x, f_y, 0]^T$ was x- and y-component of translational force vector acting at CoP from athlete's shoe. Note that all vectors in Eq. (1) were expressed in the forceplate coordinate system. The FM vector $\boldsymbol{\tau}_{\text{frc}}$ was then transformed into the global coordinate system (GCS) for subsequent inverse dynamics calculation (see, Figure 1B for the orientation of GCS).

The kinematic model consisted of foot (i = 1) and shank (i = 2) segment with ankle (j = 1) and knee (j = 2) joint was constructed (Figure 2A). The position vector of ankle joint centre (AJC) $\boldsymbol{x}_1$ was calculated as the mid-point of medial and lateral malleoli markers and the position vector of the knee joint centre (KJC) $\boldsymbol{x}_2$ was calculated as the mid-point of medial and lateral femoral epicondyle makers. The z-axis of the shank coordinate system (SCS) was defined as a unit vector $\boldsymbol{e}_z$ going from AJC to KJC, pointing proximally. The x-axis of SCS was defined as a unit vector $\boldsymbol{e}_x$ which was perpendicular to $\boldsymbol{e}_z$ and intersecting the tibial tuberosity marker, pointing anteriorly. The y-axis of the SCS was calculated as $\boldsymbol{e}_y = \boldsymbol{e}_z \times \boldsymbol{e}_x$, pointing left-side of the participant (common for both leg). The position vector of the segmental gravity centre (CoG) $\boldsymbol{x}_{g,i}$, segmental mass m_i as well as the inertia tensor $\boldsymbol{I}_i$ (foot:i = 1, shank:i = 2) were approximated referring to the Japanese athlete model (Ae

et al., 1992). The mass of shoes (0.34 kg) was added to the foot segment's mass. The foot segment's inertia tensor was also adjusted with respect to the additional mass of shoes. The position vector to CoP $\boldsymbol{x}_{\text{CoP}}$ and the GRF vector $\boldsymbol{f}$ were obtained from the forceplate data. The gravity acceleration vector was defined as $\boldsymbol{g} = [0, 0, -9.81]^T$. Although not included in the kinematic model, the position vector of mid-point of three pelvic markers (right and left ASISs, and mid-point of PSISs, Figure 1A) $\boldsymbol{x}_{\text{Pelvis}}$ and its velocity vector $\dot{\boldsymbol{x}}_{\text{Pelvis}}$ were calculated for the offline assessment of the approach speed $\|\dot{\boldsymbol{x}}_{\text{Pelvis}}\|$ and cutting angle. The cutting angle was defined as the horizontal direction of the velocity vector $\dot{\boldsymbol{x}}_{\text{Pelvis}}$ relative to the approach line (Vanrenterghem et al., 2012). For the quantification of foot-strike pattern in the offline data processing process, we assessed the orientation of the moment arm vector $\boldsymbol{r}_{2,\text{CoP}}$ going from knee joint centre to the CoP relative to the shank segment's x-axis unit vector $\boldsymbol{e}_x$. When the sign of the inner product between two vectors was $\boldsymbol{e}_x^T \boldsymbol{r}_{2,\text{CoP}} > 0$ at initial foot contact, the CoP was at anterior to the shank longitudinal axis and that trial was classified as forefoot strike, otherwise $\boldsymbol{e}_x^T \boldsymbol{r}_{2,\text{CoP}} < 0$, it was classified as rearfoot strike (Ogasawara et al., 2020). The results of the online monitoring by the two experimenters and the offline numerical foot-strike pattern classification perfectly matched.

The resultant moment vector of joint j $\boldsymbol{\tau}_{\text{res},j}$ was calculated as the resultant sum of the rotational inertia torque, gyroscopic torque, moment of linear inertia force, moment due to gravity, moment of GRF, and moment due to friction torque as (Figure 2B),

(A) Kinematic model   (B) Free body diagram

(C) Projection of moment vectors onto tibial axis.

→ Position vector
→ Linear force vector
⇒ Moment vector
⇢ Moment arm vector
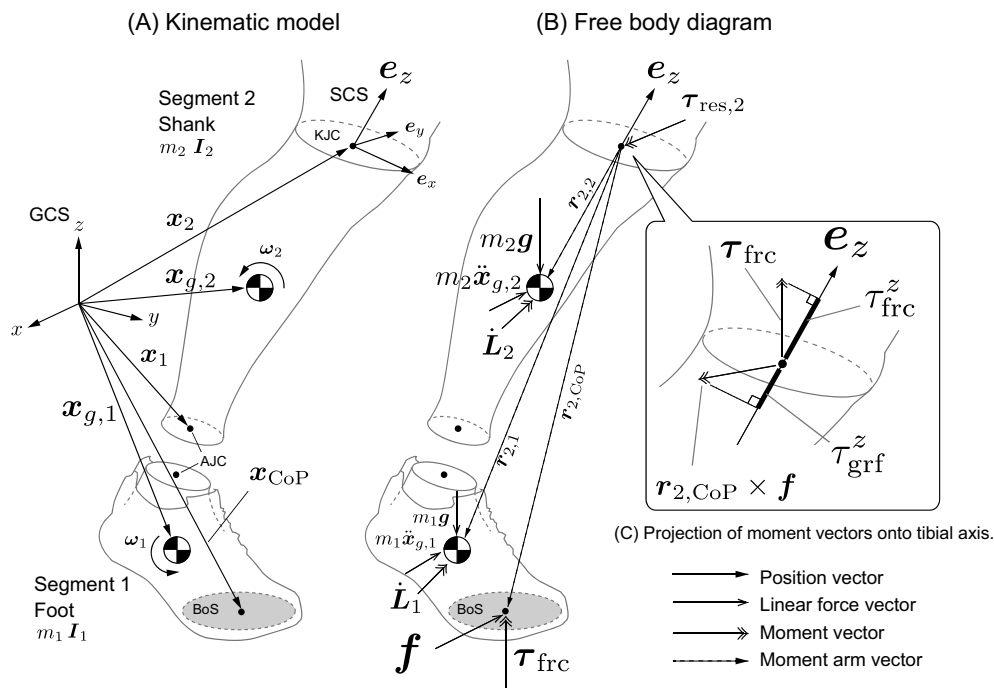
Figure 2. Kinematic model and free body diagram. The kinematic model consisting of two segments (foot and shank) and two joints (Ankle and Knee) was constructed (A). The free body diagram visually explains the Newton-Euler's equation of motion (B, Eq. (2)). Where $\dot{L}_i = I_i\dot{\omega}_i + \omega_i \times I_i\omega_i$. Only z-axis of shank coordinate system was shown for visibility. Projection of moment vectors (moment of GRF and FM) were calculated to extract effective component for tibial rotation (C).

$$\boldsymbol{\tau}_{res,j} = \sum_{i=1}^{j} \left(\boldsymbol{I}_i \dot{\boldsymbol{\omega}}_i + \boldsymbol{\omega}_i \times \boldsymbol{I}_i \boldsymbol{\omega}_i \right) + \sum_{i=1}^{j} \left(\boldsymbol{r}_{j,i} \times m_i (\ddot{\boldsymbol{x}}_{g,i} - \boldsymbol{g}) \right) \quad (2)$$
$$- \boldsymbol{r}_{j,CoP} \times \boldsymbol{f} - \boldsymbol{\tau}_{frc}, (j = 1, 2)$$

where $\boldsymbol{\omega}_i$ is the segmental angular velocity vector of segment i, and

$$\boldsymbol{r}_{j,i} = \boldsymbol{x}_{g,i} - \boldsymbol{x}_j, (j \geq i, j = 1, 2) \quad (3)$$

is the moment arm vector going from joint j to the CoG of the distal segment i, and

$$\boldsymbol{r}_{j,CoP} = \boldsymbol{x}_{CoP} - \boldsymbol{x}_j, (j = 1, 2) \quad (4)$$

is the moment arm vector going from joint j to the CoP. This resultant moment was the moment derived from the joint structures such as muscles or ligaments in response to the externally applied forces and moments (so called internal per-spective moment (Derrick et al., 2020)).

The GRF-driven internal(+)/external(−) tibial rotation moment acting at KJC was expressed as a vector projection of the moment of GRF onto the shank axis $\boldsymbol{e}_z$ as (Figure 2C),

$$\tau_{grf}^z = \boldsymbol{e}_z^T \left(\boldsymbol{r}_{2,CoP} \times \boldsymbol{f} \right) \quad (5)$$

and similarly, the FM-driven internal(+)/external(−) tibial rotation moment acting at KJC was

$$\tau_{frc}^z = \boldsymbol{e}_z^T \boldsymbol{\tau}_{frc} \quad (6)$$

For the right knee, when $\tau_{frc}^z, \tau_{grf}^z > 0$, these moments rotate the tibia towards internal direction while $\tau_{frc}^z, \tau_{grf}^z < 0$, external direction. For the consistency of the anatomical representation between legs, we multiplied −1 with the left leg's value to switch its sign.

Time-series regression between τ_{frc}^z and τ_{grf}^z to test the correlation

To obtain the time-series regression slope $\beta(n)$ between the GRF-driven tibial rotation moment τ_{grf}^z and FM-driven tibial rotation moment τ_{frc}^z, a linear regression model:

$$\boldsymbol{\tau}_{frc,n}^z = \beta_n \boldsymbol{\tau}_{grf,n}^z + a_n (n = 0 \cdots 100) \quad (7)$$

was fit to a two-dimensional (2D) scatterplot space spanned by τ_{grf}^z and τ_{frc}^z in a frame-wise manner (0 to 100%) for each leg and each foot-strike pattern. Data vectors $\boldsymbol{\tau}_{frc,n}^z$ and $\boldsymbol{\tau}_{grf,n}^z$ in Eq. (7) were moment data vectors of a given leg at n-th % stance phase from all 10 trials. This procedure was performed for each foot-strike pattern separately to obtain time-series slope $\beta(n)$ for each leg. For the meaningful interpretation of slope $\beta(n)$, each regression model fitting should meet the following assumptions, 1) Linearity between the independent and dependent data, 2) Normality of residuals, 3) Homoscedasticity of residuals, and 4) Independence of residuals. The regression diagnosis regarding above 4 assumptions were investigated for all 4,646 regression fittings by 1) R^2 (coefficient of determination), 2) Shapiro-Wilk test, 3) Breusch-Pagan test, and 4) Durbin-Watson test, respectively.

Then the time-series slope $\beta(n)$ for all 46 legs of given foot-strike pattern was input into statistical parametric mapping (SPM, (Pataky, 2012)) one sample t-test to obtain SPM

{n} curves to determine the time range where the time-series slope $\beta(n)$ value was significantly different from zero. ($p < 0.05$)

Orientation coupling (combination of moments directions) distribution between τ_{grf}^z and τ_{frc}^z

To further test the hypothesis that the FM-driven tibial rotation moment τ_{frc}^z opposes the GRF-driven moment τ_{grf}^z, we investigated the combination of orientations of those moments (positive/negative relationship) in the 2D scatterplot space defined by the τ_{grf}^z and τ_{frc}^z in a frame-wise manner. Depending on the combination of their signs (positive/negative), a data point at n-th % time frame defined by $\boldsymbol{p}_n = \left[\tau_{grf,n}^z, \tau_{frc,n}^z \right]^T$ will locate one of four quadrants of the 2D scatterplot space as

$$\boldsymbol{p}_n \in \begin{cases} 1^{st} \text{quadrant}, & \tau_{grf,n}^z > 0 \ \& \ \tau_{frc,n}^z > 0 \\ 2^{nd} \text{quadrant}, & \tau_{grf,n}^z < 0 \ \& \ \tau_{frc,n}^z > 0 \\ 3^{rd} \text{quadrant}, & \tau_{grf,n}^z < 0 \ \& \ \tau_{frc,n}^z < 0 \\ 4^{th} \text{quadrant}, & \tau_{grf,n}^z > 0 \ \& \ \tau_{frc,n}^z < 0. \end{cases} \quad (8)$$

We created a total of 101 ($n = 0$ to 100%) scatterplot spaces throughout the stance phase and distributed all the data of all trials from all legs in a frame-by-frame manner. Then we counted the number of data point for each quadrant for each frame point. The number of points were expressed as a rate of all trials. This analysis was performed separately for each foot-strike condition.

Results

Participant demographic data

Participant's mean age was 20.2 [1.3] years old, mean height was 172.9 [4.9] cm, and mean body mass was 67.8 [6.4] kg.

Approach speed, stance phase duration, and cutting angle difference between foot-strike patterns (Descriptive data in cutting motion)

There was a significant difference in the approach speeds $\|\dot{\boldsymbol{x}}_{Pelvis}\|$ between fore- and rearfoot strike condition (2.93 [0.24] m/s vs. 2.84 [0.23] m/s, Cohen d = 0.41, $p < 0.01$). The stance phase duration was significantly longer in the rearfoot strike condition than that of the forefoot strike condition (279.3 [35.3] ms vs. 298.7 [29.1] ms, Cohen d = 0.59, $p < 0.01$). The actual duration of the first 10% of stance phase for each foot-strike pattern was approx. 27.9 ms and 29.8 ms, respectively. There was no significant difference in the cutting angles between fore- and rearfoot strike condition at IC (12.4 [2.3] deg vs. 11.7 [2.2] deg, Cohen d = 0.19, p = 0.54) and at toe-off (33.8 [3.1] deg vs. 34.6 [3.0] deg, Cohen d = 0.23, p = 0.38).

Descriptive observation of time-series biomechanical variables

The friction moment (FM) expressed in the GCS (Figure 3A, 3B), the FM-driven tibial rotation moment τ_{frc}^z (Figure 3C, 3D), and due to GRF τ_{grf}^z (Figure 3E, 3F) was shown for descriptive

observation. The FM showed both positive/negative directions with high inter-trial variability throughout the stance phase for both foot-strike patterns. The FM-driven tibial rotation moment expressed in the SCS exhibited similar curve patterns to that of the FM expressed in the GCS, however, magnitudes were not identical (Figure 3A vs. 3C, 3B vs. 3D). In the rearfoot strike condition, the magnitudes of FM and FM-driven tibial rotation moment τ_{frc}^z did not become large especially first 5% stance
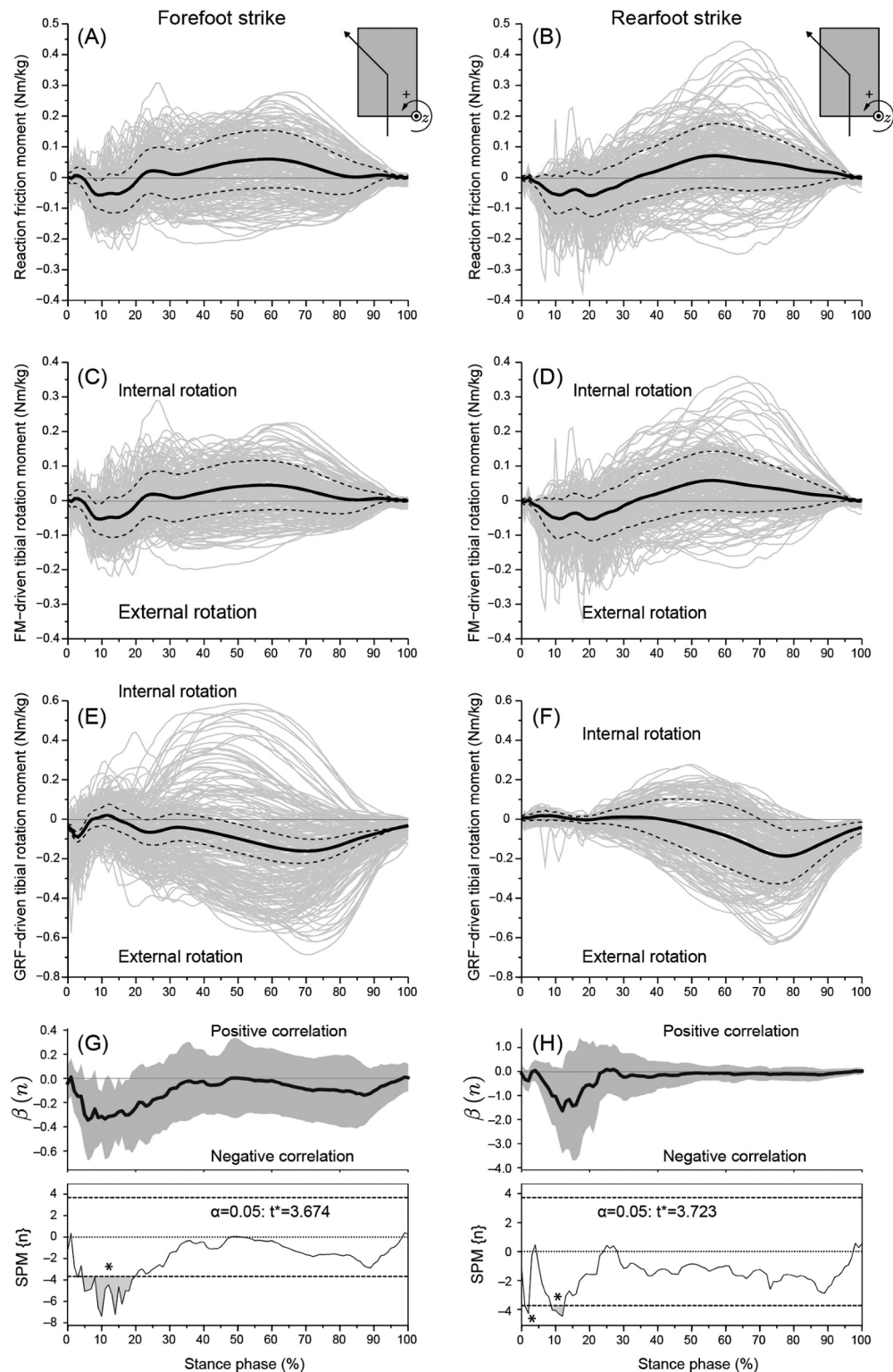

Figure 3. Time patterns of moment data and result of regression test. The FM expressed in the global coordinate system (A, B), the FM-driven (C, D) and GRF-driven (E, F) tibial rotation moment expressed in the shank coordinate system for each foot-strike pattern. The shin grey line represented each single trial of all legs. The black bold line was the ensemble averages of all trials and thin dahsed line was ± 1 standard deviation. The sign of left leg value was switched to correspond with the right leg value. Ensemble average of the 46 time-series slope $\beta(n)$ for each foot-strike pattern (black bold line) with ± 1 standard deviation (grey shaded area) and the results of SPM one-sample t-test was shown (G, H). The asterisks indicated the time duration where the time-series slope $\beta(n)$ value was significantly different from zero (p < 0.05).

phase (Figure 3B, 3D). The GRF-driven tibial rotation moment (Figure 3E, 3F) showed roughly opposite time curve to that of FM-driven tibial moment (Figure 3C, 3D) and gradually increased towards external rotation peaking round 80% of stance for both foot-strike patterns.

Regression model fitting diagnoses

1) Linearity between GRF- and FM-driven moment

65.97% (3,065/4,646) of regression models showed R^2 value of less than 0.2, indicating that the most of cases the linearity between the GRF- and FM- moment was low (Figure 4).

2) Normality of residuals

The result of the Shapiro-Wilk test ($p < 0.05$, H_0 = data is normally distributed) for the residuals of the regression models indicated that 4,295/4,646 (92.44%) models did not reject the H_0 ($p > 0.05$), suggesting that the normality of residuals is satisfied in most models.

3) Homoscedasticity of residuals

The result of the Breusch-Pagan test ($p < 0.05$, H_0 = Homoscedasticity is present) for the residuals of the regression models indicated that 4,306/4,646 (92.7%) models did not reject H_0 ($p > 0.05$), suggesting that the homoscedasticity of residuals is satisfied in most models.

4) Independence of residuals

The result of the Durbin-Watson test ($p < 0.05$, H_0 = no first order autocorrelation) for the residuals of the regression models indicated that 3,423/4,646 (75.5%) models did not reject H_0 ($p > 0.05$), suggesting that the independence of residuals are satisfied in most models.

Time-series regression between τ_{grf}^z and τ_{frc}^z to test the correlation

SPM one-sample t-test SPM{n} curves of time-series slope $\beta(n)$ revealed that the τ_{grf}^z and τ_{frc}^z showed negative correlation ($\beta < 0$) within first 20% of stance, and the ensemble averaged time-series slope $\beta(n)$ for each foot-strike pattern were significantly differ from zero (Figure 3G, 3H, $p < 0.025$). The rearfoot strikes especially showed a large negative $\beta(n)$ values at first 10% of stance phase.

Orientation coupling (combination of moments directions) distribution between τ_{grf}^z and τ_{frc}^z

For forefoot strikes, the trials distribution onto the 2nd ($\tau_{grf}^z < 0$ [external] and $\tau_{frc}^z > 0$ [internal]) and 3rd ($\tau_{grf}^z < 0$ [external] and $\tau_{frc}^z < 0$ [external]) quadrants were momentary high from 0 to 4% of the stance phase but the distribution of 4th quadrant ($\tau_{grf}^z > 0$ [internal] and $\tau_{frc}^z < 0$ [external]) increased from 5 to 20% of stance phase (Figure 5A). For rearfoot strikes, the 4th quadrant showed a high trials distribution during 0–15% of stance phase. The 1st quadrant ($\tau_{grf}^z > 0$ [internal] and $\tau_{frc}^z > 0$ [internal]) scored the lowest trials distribution from 0 to 20% of the stance phase but showed gradual increases from 20 to 50%, then decreased to 80% of stance phase for both foot-strikes. After 20% of the stance phase, the trial distribution onto the 2nd quadrant ($\tau_{grf}^z < 0$ [external] and $\tau_{frc}^z < 0$ [internal]) gradually increased towards the toe-off phase and peaked from 90 to 100% of the stance phase. A 2D scatterplot space spanned by the GRF-driven tibial rotation moment and the FM-driven tibial rotation moment at 10% of stance phase was shown for each foot-strike (Figure 5C, 5D). A large trials distribution onto the 4th quadrants was confirmed especially for rearfoot strike (Figure 5D). On the horizontal axis (GRF-driven tibial rotation moment), the forefoot strike trials were distributed over a wide range from negative (external) to positive (internal), while the rearfoot strike trials were concentrated in the positive (internal; Figure 5C, 5D). The trials which showed internal resultant tibial rotation moment (white dots) were distributed under the negative diagonal line, while the trials with the external resultant tibial rotation moment (black dots) were did above the negative diagonal line (Figure 5C, 5D).

Discussion

This is the first study that evaluated the mechanical interaction between GRF-driven and FM-driven tibial rotation moment applied at knee in an early deceleration phase of cutting manoeuvre in young male athletes. Results clearly demonstrated that the FM-driven tibial rotation moment and the GRF-driven
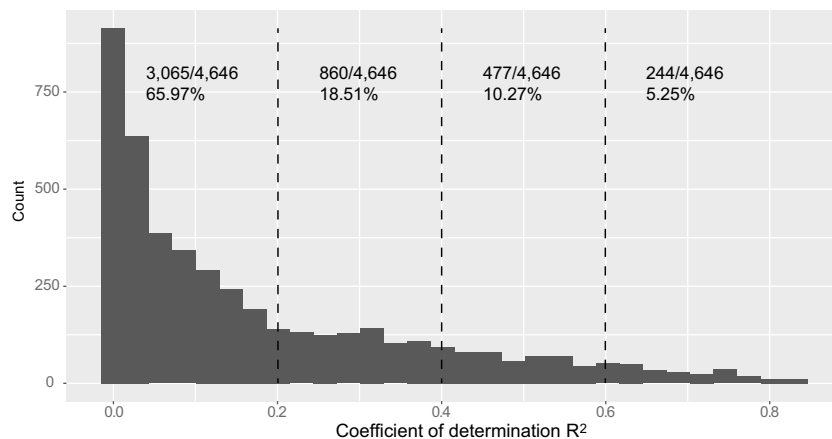

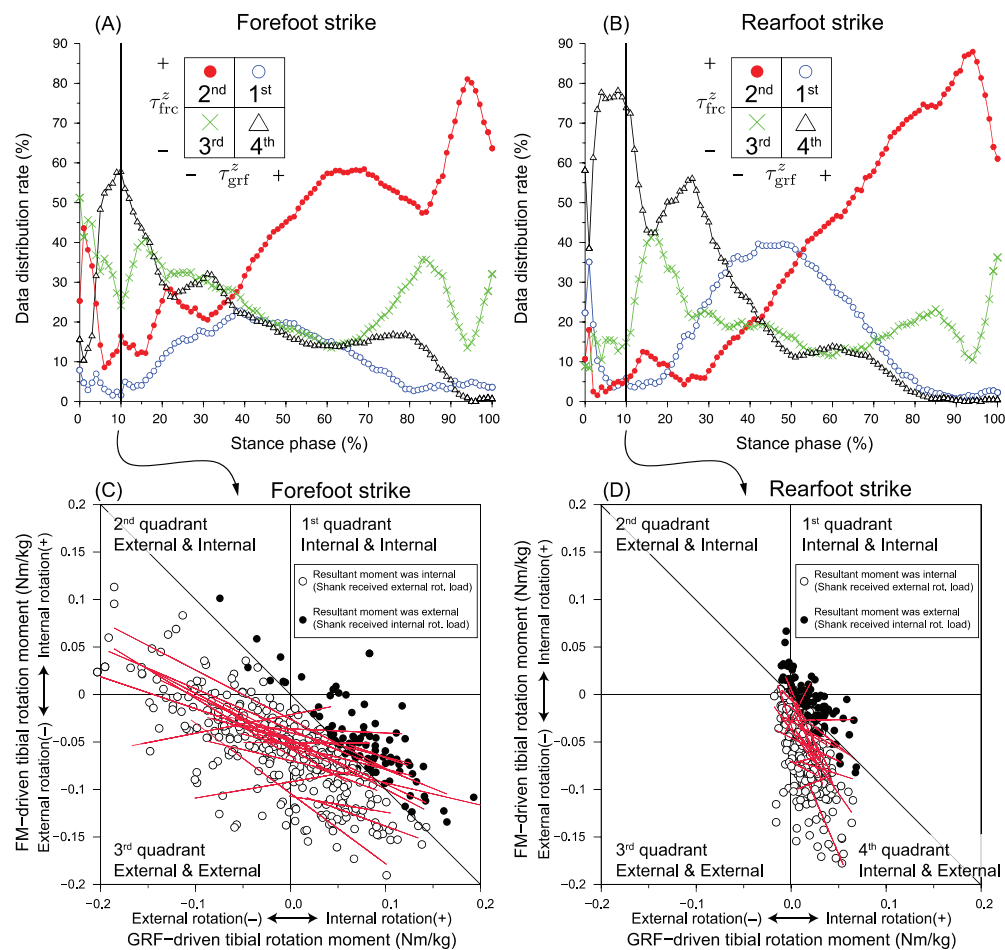**Figure 4. Histogram of R^2 for all regression model.**

Figure 5. Orientation coupling distribution between τ^z_{grf} and τ^z_{frc}. All trials were scattered onto the 2D plane spanned by and τ^z_{grf} and τ^z_{frc}, and number of trials were summed up for each quadrant separately in a frame-wise manner to investigate the time course change of the orientation coupling distribution for each foot-strikes (A, B). The representative scatterplots at 10% stance phase were shown for each foot-strikes (C, D). The white dots indicated the trial with the resultant tibial rotation moment was internal, meaning that the tibia received an external rotation load, while the black dots indicated the trial with the resultant tibial rotation moment was external, meaning that the tibia received an internal rotation load. The red lines denoted the regression slopes. (For interpretation of the references to colour in this figure legend, the reader is referred to the web version of this article).

one counteracted during the first 20% of stance phase (Figure 3G, 3H and Figure 5). These results positively supported our hypothesis that the tibial rotation moment due to GRF and due to FM are negatively correlated and the actions of those moments oppose each other at an early stance phase. Our finding was simply interpreted as follows; when the GRF is about to rotate the shank in one direction, the reactive FM acting at CoP resists that GRF-driven rotation accordingly (Figure 6A). This counteractive relationship between GRF and FM may be effective in maintaining an appropriate shank orientation during the deceleration phase of a cutting manoeuvre. The FM has been regarded as a stressor for several athletic trauma types, commonly as tibial stress fracture (Milner et al., 2006), ankle and knee injury (Wannop et al., 2010) and non-contact ACL injury (David & Potthast, 2021). However, our findings prompt the need to reconsider the role of FM, at least in the context of the mechanisms of acute noncontact ACL injuries.

The time-pattern and magnitude of FM expressed in the GCS were similar to a recent study by David et al. (2021). Despite a task difference between the studies (90° sidestepping in

David et.al and 45° cutting in our study), a high inter-trial variability in the general FM curve was consistent. In this study, the FM-driven tibial rotation moment in the SCS was similar to FM in the GCS in its curve pattern and magnitude (Figure 3). We speculated that the projection of FM vector onto tibial axis e_z was maximized when the shank was in an upright position, as predicted from Eq. (6). Interestingly, the magnitude of FM during the first 10% stance did not become large (Figure 3A, 3B), which is more typical in rearfoot strikes than in forefoot strikes (Figure 3B). Since the vertical loading and BoS contact area determine the FM magnitude (Holden & Cavanagh, 1991), a smaller heel-floor contact area may negatively contribute to FM enlargement at rearfoot impact. For GRF-driven tibial rotation moment, trials from the forefoot strikes showed a greater distribution from external to internal tibial rotation (Figure 5C), while most trials from the rearfoot strikes distributed in the internal tibial rotation (Figure 5D). This difference in the direction of GRF-driven moment between fore- and rearfoot strikes was consistently observed in previously reported female cutting motion (Ogasawara et al., 2020). Overall, the above commonalities indicate that the
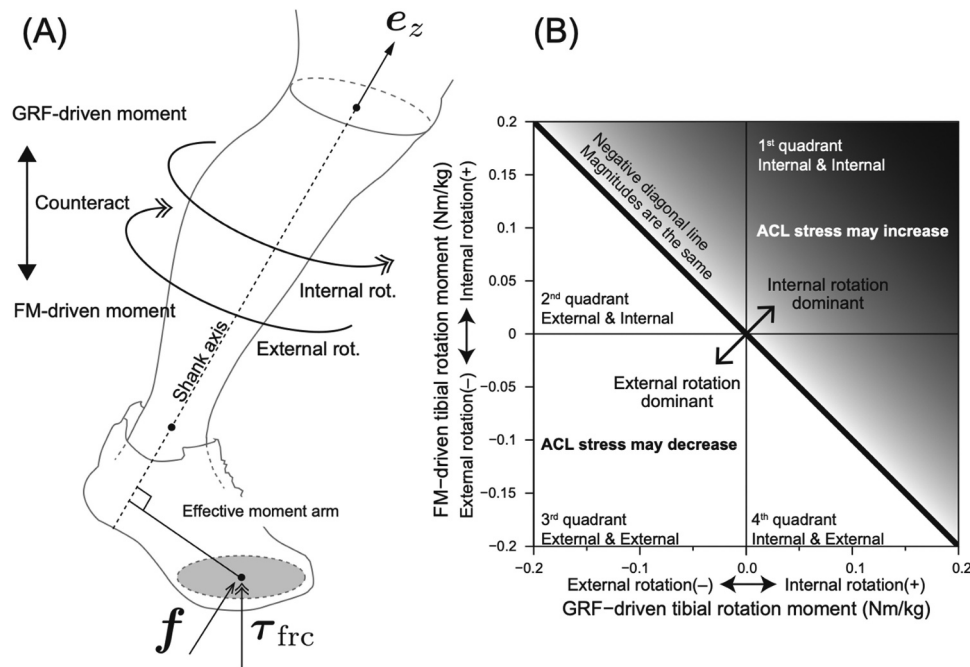
Figure 6. Schematic representation of counteracting relationship between FM and GRF at knee. The counteractive relationship between τ_{grf}^{z} and τ_{frc}^{z} (A). Physiological interpretation of orientation coupling 2D scatterplot space (B). Internal & Internal combination (1st quadrant) may increase the ACL stress while the External & External combination (3rd quadrant) may decrease the ACL stress. Opposing orientation combination (2nd and 4th quadrant) means that τ_{grf}^{z} and τ_{frc}^{z} are counteracting each other. When the trial was at above the negative diagonal line, the effect of the internal rotation moment becomes dominant relative to the external rotation moment and vice versa.

cutting task in this study was well replicated and controlled. Thus, the quality of this study was the same level as the previous studies and the results of this study were appropriate for comparison with the previous studies.

The visualization of orientation coupling of two rotational moments provided several important insights into the combined effects of τ_{grf}^{z} and τ_{frc}^{z} on the horizontal-plane knee loadings in cutting (Figure 5). Most trials distributed over 4th quadrant at the first 10% of stance phase and this trend was more prominent for rearfoot strikes than for forefoot strikes (Figure 5). This indicates that the FM-driven "external" moment counteracted the GRF-driven tibial "internal" rotation moment in most trials. Moreover, the black and white dots distributed across the negative diagonal line of the 2D scatterplot space indicated that the dynamic equilibrium between GRF- and FM-driven tibial rotation moment dominantly determined the direction of resultant tibial rotation moment (Figure 5C, 5D). The occurrence of "Internal & Internal" coupling (1st quadrant) was the lowest at the first 10% of stance phase for both foot strikes in this experiment (Figure 5A, 5B). This suggested that the high tibial internal rotation loading, which potentially increases the ACL stress, occurred the least during non-injurious cutting tasks in this experiment (Figure 6B). Though we did not observe any specific trial, the cutting manoeuvre which falls within the upper right corner of the 1st quadrant exhibits the largest tibial internal moment. It is reasonable to speculate that the actual ACL injury event may experience such a synchronized $\tau_{grf}^{z} > 0$ and $\tau_{frc}^{z} > 0$ outcome. In addition to the 4th quadrant trials, the forefoot strikes produced "External & External" coupling (3rd quadrant) trials as well at the very first

moment of foot impact (Figure 5A, 5C). In vitro studies have reported that the ACL strain (Bates et al., 2017; Oh et al., 2012) or resultant ACL force (Markolf et al., 1990) become smaller in response to the tibial external rotation moment than internal rotation moment. The "External & External" coupling observed in the forefoot strikes therefore does not necessarily represents the risk of ACL injury in the forefoot strikes (Figure 6B). Although rearfoot strikes are an at-risk landing technique to ACL injury (Boden et al., 2009; Koga et al., 2018; Montgomery et al., 2016; Ogasawara et al., 2020), one of the favourable findings of our study with regards to ACL injury prevention was that the counteracting relationship between GRF- and FM-driven tibial rotation moments worked well during the first 10% stance phase of rearfoot strikes (Figure 3H and 4D). The more inclined regression slope $\beta(n)$ at the first 10% of stance phase in rearfoot strikes explained a high sensitivity of the FM resistance in response to the GRF-driven tibial internal loading at the first 10% stance phase of rearfoot strikes (Figure 3H, Figure 5D).

Whether the FM is harmful to ACL or not is still controversial. However, we consider that a reasonable amount of reactive FM prevents the GRF-driven tibial internal rotation and may protect ACL from GRF threat after foot impact. This concept is well supported from our results that the resultant tibial rotation moment becomes the internal rotation moment when the FM-driven external rotation moment sufficiently counteracts against the GRF-driven internal rotation moment (Figure 5C, 5D). However, a careful interpretation is required to acknowledge this concept since previous literature suggest that the FM is a potential risk for knee ligamentous injury, including ACL

(David & Potthast, 2021; Wannop et al., 2010). These conclusions may be attributed to the differences in the analytical time frames. Our study focused on an early deceleration phase (so-called passive phase), where the FM magnitude is relatively small. In contrast, prior studies have mainly addressed mid to late active phase where the FM or the tibial rotation moment showed large magnitudes. Wannop et al. (2010) reported that cutting with high-traction shoes produced significantly greater peak knee internal rotation moments around 50–60% of stance phase than that of the low-traction shoe and suggested that high traction shoes may increase knee injury risk. David et al. (2021) found that cutting motions with less preorientation demanded the FM to rotate the body orientation at post foot contact phase and suggested that the increased FM along with the tibial internal rotation moment may functionally stress the ACL. That high FM magnitude at the active phase increases knee ligament stress is therefore acceptable to some extent. However, since athletes voluntarily and actively control the amount of FM and GRF to produce a proper body rotation and accelerate themselves towards the desired direction at the active phase (David & Potthast, 2021; Jindrich et al., 2006), it is debatable whether a self-produced reactive FM will become unsafe for the ACL. Furthermore, in the active phase, the knee muscles also dynamically account for the demand of external knee loadings, and not solely stressing the passive structures (Buchanan et al., 1996; Lloyd & Buchanan, 2001). Therefore, the increased FM in the mid to late stance phase is unlikely to endanger the ACL, with the fact that non-contact ACL injury frequently occurs soon after foot strikes (Koga et al., 2011). The reported time frame for ACL injury was approximately the first 40 ms after IC (Koga et al., 2010), where the FM magnitude was not found to be high enough and this trend was more prominent for the rearfoot strikes (Figure 3). ACL injuries often occur just after heel impact (Boden et al., 2009; Koga et al., 2018; Montgomery et al., 2016), where the magnitude of FM does not increase sufficiently. It may therefore be reasonable to posit that a sufficient amount of FM contributes to ACL protection.

As a practical implication of this study in the context of ACL injury, we consider it is essential to establish a rotationally stable BoS at the very beginning of deceleration phase. Due to the high variability in FM magnitude, an intentional control of FM may not be simple. However, one practical technique to emphasize the merit of FM is to use forefoot landing. The forefoot landing with a wide BoS area would be advantageous for producing large FM at the very beginning of deceleration phase as compared to rearfoot strike (Figure 3A, 3B). The upright shank orientation also contributes to maximize the projection of FM vector onto the tibial axis (Eq. (6), Figure 7A). In this regard, the previously suggested "provocative posture" by Boden et al. (2009) may impair the benefit of FM as this posture consists of heel edge strike with a posterior inclined shank orientation (Figure 7B). Use of forefoot landing is also recommended since the significantly faster approach speed and shorter stance duration found in forefoot trials were mechanical determinants of a faster change of direction performance in sports (Dos'Santos et al., 2019, 2017;

Welinski et al., 2021). Literature on FM-related ACL injury mechanism and ACL protection mechanism are few and incorporating the merit of FM in injury prevention programmes is the subject of a future study. The role of FM should be separately discussed at foot impact phase and active phase even in one cutting motion sequence. Elucidating the importance of FM for dynamic rotational equilibrium of the stance limb, especially before ACL injury (less than 40 ms after IC (Koga et al., 2010)), will provide an insight into injury mechanisms as well as the risk reduction of non-contact ACL injury.

This study had several limitations. Since this study recruited male participants only, a cautious interpretation is needed to generalize our findings to female athletes. To eliminate the potential effect of known sex-disparity in cutting biomechanics (Pollard et al., 2007; Sigward & Powers, 2006), this study adopted a single-sex design. Although the high ACL injury rate in female athletes is indeed a concern, many ACL injuries occurring in male athletes are also troublesome (Agel et al., 2016; Mountcastle et al., 2007; Røtterud et al., 2011). Since there have been fewer studies describing ACL injury mechanisms in men, specific studies such as ours are expected to contribute towards the prevention and management of ACL injuries in men. For the participants' safety, we used a relatively slow approach speed range. This was ethically important but may have reduced the ecological validity in terms of knee loading magnitude because the absolute knee moment magnitude in real sporting conditions is expected to be much higher. However, our findings in this study i.e., negative correlation or orientation coupling between τ_{grf}^z and τ_{frc}^z, were fundamentally different from the magnitude-based risk representation which have been adopted by the most of lab-controlled studies so far. We believe biomechanical risk for ACL injury should be discussed not only in terms of loading magnitude but also with respect to the interaction of several moment orientations. Therefore, the importance of our conclusion may not be depreciated solely by the slow approach speed. Kristianslund et al. (2012) suggested that the GRF signal should be low-pass filtered with the same low cut-off frequency as the marker data to coincide with the frequency components
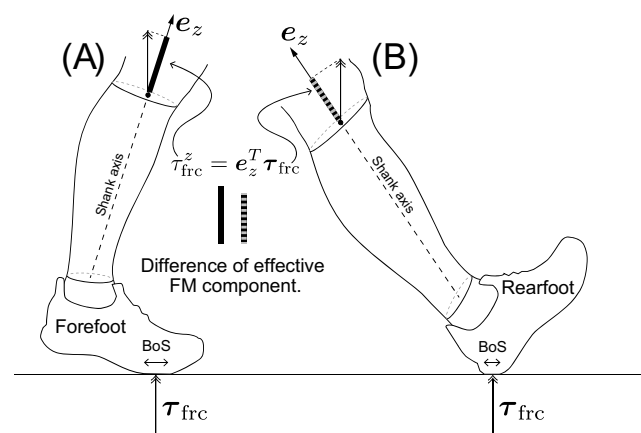

Figure 7. **Difference on the effective FM component between fore- and rearfoot strike**. Length of FM vector projection onto the shank axis varies depending on the shank orientation. More posterior inclined shank orientation decreases the FM vector projection length.

involved in both signals. However, they only investigated the effect of identical cut-off filtering frequency with the discrete peak knee valgus moment and did not generalize neither in FM nor FM-driven tibial rotation moment. In this study, we smoothed GRF signal with the cut-off frequency of 70 Hz only to eliminate the quantization noise produced in analog-to-digital converting process. The aim of this study was to investigate the orientation coupling of FM- and GRF-driven tibial rotation moment in cutting and not to rate the participants with their biomechanical variables, which is sensitive to the cut-off frequency choice (Kristianslund et al., 2012). Further study will be required to determine the optimal filtering methodology for the inverse dynamics. Most regression model fitting (3,065/4,646, 66.0%, Figure 4) resulted in low R^2 values of less than 0.2 although the other assumptions (Normality of residuals, the homoscedasticity of residuals, and the independence of residuals) were mostly met. This finding is mechanically well expected that the values of GRF-driven τ_{grf}^z and FM-driven moment τ_{frc}^z are mutually affected by the other moment terms, e.g., the moment of translational/rotational inertia, the moment of gravity, the gyroscopic torque, and the moments derived from the joint structures as formulated by the equation of motion (Eq. (2), (Ogasawara et al., 2021)). The nonlinear relationship among the different moment terms in Eq. (2) reduced the linearity between GRF-driven τ_{grf}^z and FM-driven moments τ_{frc}^z and might be a concern for the validity of the slope $\beta(n)$ value. However, the slope $\beta(n)$ value averaged over all participants showed a systematic negatively-oriented trend during the first 20% of the stance phase for each foot-strike condition (Figure 3G, 3H). In addition, our hypothesis, that the directions of the GRF-driven τ_{grf}^z and FM-driven moments τ_{frc}^z oppose each other at an early stance phase of cutting, was also supported by the results of the orientation coupling assessment between τ_{grf}^z and τ_{frc}^z (Figure 5). Therefore, one of the statistical characteristics regarding the relationship between GRF-driven τ_{grf}^z and FM-driven moment τ_{frc}^z, that is, the low linearity, solely does not discard the mechanical findings of this study nor alter our conclusion. Since we expected that the coefficient of friction between shoe sole and force-plate's surface potentially differentiate the magnitude of FM and FM-driven tibial rotation moment, we used the newly prepared the same model of shoe among participants. This methodological control minimized the inter-participant variability of FM-related variables due to the coefficient of friction variability. However, note that the magnitudes of FM and FM-induced tibial rotation moment observed in this study was specific to our equipment (shoes and force-plate's surface). The different combination of shoe model and force-plate surface potentially returns the different magnitude of FM.

Conclusion

This human experimental study identified that the tibial rotational moments driven by GRF and by FM in an early stance phase of cutting manoeuvre counteracted each other in both forefoot and rearfoot strikes in male athletes. The counteracting effect of FM-driven tibial rotation moment against the GRF-driven one may positively contribute to maintain the appropriate shank orientation of stance limb at the foot impact phase and may relieve knee rotational loading by the GRF.

Abbreviations

ACL	anterior cruciate ligament
GRF	ground reaction force
BoS	base of support
3D	three dimensional
FM	friction moment
CoP	center of pressure
SCS	shank coordinate system
GCS	global coordinate system
AJC	ankle joint center
KJC	knee joint center
CoG	center of gravity
SPM	statistical parametric mapping

ORCID

Issei Ogasawara 🆔 http://orcid.org/0000-0003-4176-689X
Yuki Uno 🆔 http://orcid.org/0000-0003-1579-2736
Gajanan S. Revankar 🆔 http://orcid.org/0000-0002-3753-4140
Shoji Konda 🆔 http://orcid.org/0000-0002-8252-7281
Tomoyuki Matsuo 🆔 http://orcid.org/0000-0002-9356-7406

References

Ae, M., Tang, H. P., & Yokoi, T. (1992). Estimation of inertia properties of the body segments in Japanese athletes. *Biomechanism*, *11*, 23–33. https://doi.org/10.3951/biomechanisms.11.23

Agel, J., Rockwood, T., & Klossner, D. (2016). Collegiate ACL injury rates across 15 sports: National collegiate athletic association injury surveillance system data update (2004-2005 through 2012-2013). *Clinical Journal of Sport Medicine: Official Journal of the Canadian Academy of Sport Medicine*, *26*(6), 518–523. https://doi.org/10.1097/JSM.0000000000000290

Ardern, C. L., Taylor, N. F., Feller, J. A., & Webster, K. E. (2014). Fifty-five per cent return to competitive sport following anterior cruciate ligament reconstruction surgery: An updated systematic review and meta-analysis including aspects of physical functioning and contextual factors. *British Journal of Sports Medicine*, *48*(21), 1543. https://doi.org/10.1136/bjsports-2013-093398

Arendt, E., & Dick, R. (1995). Knee injury patterns among men and women in collegiate basketball and soccer. *American Journal of Sports Medicine*, *23*(6), 694–701. https://doi.org/10.1177/036354659502300611

Bates, N. A., Nesbitt, R. J., Shearn, J. T., Myer, G. D., & Hewett, T. E. (2017). Knee abduction affects greater magnitude of change in ACL and MCL strains than matched internal tibial rotation in vitro. *Clinical Orthopaedics and Related Research*, *475*(10), 2385–2396. https://doi.org/10.1007/s11999-017-5367-9

Biedert, R. M., & Zwick, E. B. (1998). Ligament-muscle reflex arc after anterior cruciate ligament reconstruction: Electromyographic evaluation. *Archives of Orthopaedic and Trauma Surgery*, *118*(1–2), 81–84. https://doi.org/10.1007/s004020050317

Boden, B. P., Breit, I., & Sheehan, F. T. (2009). Tibiofemoral alignment: Contributing factors to noncontact anterior cruciate ligament injury. *Journal of Bone and Joint Surgery American Volume*, 91(10), 2381–2389. https://doi.org/10.2106/JBJS.H.01721

Boden, B. P., Dean, G. S., Feagin, J. A. J., & Garrett, W. E. J. (2000). Mechanisms of anterior cruciate ligament injury. *Orthopedics*, 23(6), 573–578. https://doi.org/10.3928/0147-7447-20000601-15

Boden, B. P., Torg, J. S., Knowles, S. B., & Hewett, T. E. (2009). Video analysis of anterior cruciate ligament injury. *American Journal of Sports Medicine [Internet]*, 37, 252–259. Available from http://journal.ajsm.org/cgi/doi/10.1177/0363546508328107

Buchanan, T. S., Kim, A. W., & Lloyd, D. G. (1996). Selective muscle activation following rapid varus/valgus perturbations at the knee. *Medicine and Science in Sports and Exercise*, 28(7), 870–876. https://doi.org/10.1097/00005768-199607000-00014

David, S., & Potthast, W. (2021). Control strategies during fast turning manoeuvers - the free moment and its contribution to body rotation and joint loading. *Journal of Sports Science*, 39(24), 2812–2820. https://doi.org/10.1080/02640414.2021.1964748

Derrick, T. R., van den, B. A. J., Cereatti, A., Dumas, R., Fantozzi, S., & Leardini, A. (2020). ISB recommendations on the reporting of intersegmental forces and moments during human motion analysis. *Journal of Biomechanics*, 99, 109533. https://doi.org/10.1016/j.jbiomech.2019.109533

Dos'Santos, T., McBurnie, A., Thomas, C., Comfort, P., & Jones, P. A. (2019). Biomechanical determinants of the modified and traditional 505 change of direction speed test. *Journal of Strength and Conditioning Research / National Strength & Conditioning Association*, 34(5), 1285–1296. https://doi.org/10.1519/JSC.0000000000003439

Dos'Santos, T., Thomas, C., Jones, P. A., & Comfort, P. (2017). mechanical determinants of faster change of direction speed performance in male athletes. *Journal of Strength and Conditioning Research / National Strength & Conditioning Association*, 31(3), 696–705. https://doi.org/10.1519/JSC.0000000000001535

Friemert, B., Faist, M., Spengler, C., Gerngross, H., Claes, L., & Melnyk, M. (2005). Intraoperative direct mechanical stimulation of the anterior cruciate ligament elicits short- and medium-latency hamstring reflexes. *Journal of Neurophysiology*, 94(6), 3996–4001. https://doi.org/10.1152/jn.00410.2005

Grevnerts, H. T., Sonesson, S., Gauffin, H., Ardern, C. L., Stålman, A., & Kvist, J. (2021). Decision making for treatment after ACL injury from an orthopaedic surgeon and patient perspective: results from the NACOX study. *Orthopaedic Journal of Sports Medicine*, 9(4), 23259671211005090. https://doi.org/10.1177/23259671211005090

Griffin, L. Y., Agel, J., Albohm, M. J., Arendt, E. A., Dick, R. W., Garrett, W. E., Garrick, J. G., Hewett, T. E., Huston, L., Ireland, M. L., Johnson, R. J., Kibler, W. B., Lephart, S., Lewis, J. L., Lindenfeld, T. N., Mandelbaum, B. R., Marchak, P., Teitz, C. C., & Wojtys, E. M. (2000). Noncontact anterior cruciate ligament injuries: Risk factors and prevention strategies. *Journal of the American Academy of Orthopaedic Surgeons*, 8(3), 141–150. https://doi.org/10.5435/00124635-200005000-00001

Holden, J. P., & Cavanagh, P. R. (1991). The free moment of ground reaction in distance running and its changes with pronation. *Journal of Biomechanics*, 24(10), 887–897. https://doi.org/10.1016/0021-9290(91)90167-L

Ireland, M. L. (1999). Anterior cruciate ligament injury in female athletes: Epidemiology. *Journal of Athletic Training [Internet]*, 34, 150–154. Available from http://www.ncbi.nlm.nih.gov/sites/entrez?Db=pubmed&Cmd=Retrieve&list_uids=16558558&dopt=abstractplus

Jindrich, D. L., Besier, T. F., & Lloyd, D. G. (2006). A hypothesis for the function of braking forces during running turns. *Journal of Biomechanics*, 39(9), 1611–1620. https://doi.org/10.1016/j.jbiomech.2005.05.007

Koga, H., Bahr, R., Myklebust, G., Engebretsen, L., Grund, T., & Krosshaug, T. (2011). Estimating anterior tibial translation from model-based image-matching of a noncontact anterior cruciate ligament injury in professional football: A case report. *Clinical Journal of Sport Medicine: Official Journal of the Canadian Academy of Sport Medicine*, 21(3), 271–274. https://doi.org/10.1097/JSM.0b013e31821899ec

Koga, H., Nakamae, A., Shima, Y., Bahr, R., & Krosshaug, T. (2018). Hip and ankle kinematics in noncontact anterior cruciate ligament injury situations: video analysis using model-based image matching. *American Journal of Sports Medicine*, 46(2), 333–340. https://doi.org/10.1177/0363546517732750

Koga, H., Nakamae, A., Shima, Y., Iwasa, J., Myklebust, G., Engebretsen, L., Bahr, R., Krosshaug, T., Koga, H., Nakamae, A., Shima, Y., Bahr, R., & Krosshaug, T. (2010). Mechanisms for noncontact anterior cruciate ligament injuries. *American Journal of Sports Medicine*, 38(11), 2218–2225. https://doi.org/10.1177/0363546510373570

Kristianslund, E., Faul, O., Bahr, R., Myklebust, G., & Krosshaug, T. (2014). Sidestep cutting technique and knee abduction loading: Implications for ACL prevention exercises. *British Journal of Sports Medicine*, 48(9), 779–783. https://doi.org/10.1136/bjsports-2012-091370

Kristianslund, E., Krosshaug, T., & van den, B. A. J. (2012). Effect of low pass filtering on joint moments from inverse dynamics: Implications for injury prevention. *Journal of Biomechanics*, 45, 666–671. https://doi.org/10.1016/j.jbiomech.2011.12.011

Krosshaug, T., Nakamae, A., Boden, B. P., Engebretsen, L., Smith, G., Slauterbeck, J. R., Hewett, T. E., & Bahr, R. (2007). Mechanisms of anterior cruciate ligament injury in basketball: video analysis of 39 cases. *American Journal of Sports Medicine*, 35(3), 359–367. https://doi.org/10.1177/0363546506293899

Lloyd, D. G., & Buchanan, T. S. (2001). Strategies of muscular support of varus and valgus isometric loads at the human knee. *Journal of Biomechanics*, 34(10), 1257–1267. https://doi.org/10.1016/s0021-9290(01)00095-1

Lohmander, L. S., Ostenberg, A., Englund, M., & Roos, H. (2004). High prevalence of knee osteoarthritis, pain, and functional limitations in female soccer players twelve years after anterior cruciate ligament injury. *Arthritis and Rheumatology*, 50(10), 3145–3152. https://doi.org/10.1002/art.20589

Markolf, K. L., Burchfield, D. M., Shapiro, M. M., Shepard, M. F., Finerman, G. A., & Slauterbeck, J. L. (1995). Combined knee loading states that generate high anterior cruciate ligament forces. *Journal of Orthopaedic Research [Internet]*, 13, 930–935. Available from http://eutils.ncbi.nlm.nih.gov/entrez/eutils/elink.fcgi?dbfrom=pubmed&id=8544031&retmode=ref&cmd=prlinks

Markolf, K. L., Gorek, J. F., Kabo, J. M., & Shapiro, M. S. (1990). Direct measurement of resultant forces in the anterior cruciate ligament. An in vitro study performed with a new experimental technique. *The Journal of Bone and Joint Surgery American*, (72), 557–567. Internet];:. Available from http://eutils.ncbi.nlm.nih.gov/entrez/eutils/elink.fcgi?dbfrom=pubmed&id=2324143&retmode=ref&cmd=prlinks

McLean, S. G., Huang, X., & van den, B. A. J. (2005). Association between lower extremity posture at contact and peak knee valgus moment during sidestepping: Implications for ACL injury. *Clinical Biomechanics*, 20(8), 863–870. https://doi.org/10.1016/j.clinbiomech.2005.05.007

Meyer, E., Baumer, T., Slade, J., Smith, W., & Haut, R. C. (2008). Tibiofemoral contact pressures and osteochondral microtrauma during ACL rupture due to excessive compressive loading and internal torque of the human. *The American Journal of Sports Medicine*, 36(10), 1966–1977. https://doi.org/10.1177/0363546508318046

Meyer, E. G., & Haut, R. C. (2005). Excessive compression of the human tibio-femoral joint causes ACL rupture. *Journal of Biomechanics*, 38(11), 2311–2316. https://doi.org/10.1016/j.jbiomech.2004.10.003

Meyer, E. G., & Haut, R. C. (2008). Anterior cruciate ligament injury induced by internal tibial torsion or tibiofemoral compression. *Journal of Biomechanics*, 41(16), 3377–3383. https://doi.org/10.1016/j.jbiomech.2008.09.023

Milner, C. E., Davis, I. S., & Hamill, J. (2006). Free moment as a predictor of tibial stress fracture in distance runners. *Journal of Biomechanics*, 39(15), 2819–2825. https://doi.org/10.1016/j.jbiomech.2005.09.022

Montgomery, C., Blackburn, J., Withers, D., Tierney, G., Moran, C., & Simms, C. (2016). Mechanisms of ACL injury in professional rugby union: A systematic video analysis of 36 cases. *British Journal of Sports Medicine*, 52(15), 994–1001. https://doi.org/10.1136/bjsports-2016-096425

Mountcastle, S. B., Posner, M., Kragh, J. F., & Taylor, D. C. (2007). Gender differences in anterior cruciate ligament injury vary with activity.

American Journal of Sports Medicine, 35(10), 1635–1642. https://doi.org/10.1177/0363546507302917

Ogasawara, I., Shimokochi, Y., Konda, S., Mae, T., & Nakata, K. (2021). Effect of rearfoot strikes on the hip and knee rotational kinetic chain during the early phase of cutting in female athletes. *Sports Medicine - Open*, 7(1), 75. https://doi.org/10.1186/s40798-021-00368-w

Ogasawara, I., Shimokochi, Y., Mae, T., & Nakata, K. (2020). Rearfoot strikes more frequently apply combined knee valgus and tibial internal rotation moments than forefoot strikes in females during the early phase of cutting maneuvers. *Gait & Posture*, 76, 364–371. https://doi.org/10.1016/j.gaitpost.2019.11.014

Oh, Y. K., Kreinbrink, J. L., Wojtys, E. M., & Ashton-Miller, J. A. (2012). Effect of axial tibial torque direction on ACL relative strain and strain rate in an in vitro simulated pivot landing. *Journal of Orthopaedic Research*, 30(4), 528–534. https://doi.org/10.1002/jor.21572

Oh, Y. K., Lipps, D. B., Ashton-Miller, J. A., & Wojtys, E. M. (2012). What strains the anterior cruciate ligament during a pivot landing? *American Journal of Sports Medicine*, 40(3), 574–583. https://doi.org/10.1177/0363546511432544

Pataky, T. C. (2012). One-dimensional statistical parametric mapping in Python. *Computer Methods in Biomechanics*, 15(3), 295–301. https://doi.org/10.1080/10255842.2010.527837

Pollard, C. D., Sigward, S. M., & Powers, C. M. (2007). Gender differences in hip joint kinematics and kinetics during side-step cutting maneuver. *Clinical Journal of Sport Medicine: Official Journal of the Canadian Academy of Sport Medicine*, 17(1), 38–42. https://doi.org/10.1097/JSM.0b013e3180305de8

Prodromos, C. C., Han, Y., Rogowski, J., Joyce, B., & Shi, K. (2007). A meta-analysis of the incidence of anterior cruciate ligament tears as a function of gender, sport, and a knee injury–reduction regimen. *Arthroscopy - Journal of Arthroscopic and Related Surgery*, 23(12), 1320–1325.e6. https://doi.org/10.1016/j.arthro.2007.07.003

Quatman, C. E., Quatman-Yates, C. C., & Hewett, T. E. (2010). A 'plane' explanation of anterior cruciate ligament injury mechanisms. *Sports Medicine*, 40(9), 729–746. https://doi.org/10.2165/11534950-000000000-00000

Robinson, M., & Donnelly, C. (2017). *An exploratory analysis correlating force plate free moments and multi- component knee moments during sidestepping* [Paper presentation]. The XXVI Congress of the International Society of Biomechanics, Jul 23–27, Brisbane, Australia, p71. [cited 2022 Jan 14]. Available from: https://media.isbweb.org/images/conferences/isb-congresses/2017/ISB2017-Full-Abstract-Book.pdf

Røtterud, J. H., Sivertsen, E. A., Forssblad, M., Engebretsen, L., & Årøen, A. (2011). Effect of gender and sports on the risk of full-thickness articular cartilage lesions in anterior cruciate ligament-injured knees: A nationwide cohort study from Sweden and Norway of 15 783 patients. *American Journal of Sports Medicine*, 39(7), 1387–1394. https://doi.org/10.1177/0363546510397813

Sakane, M., Fox, R. J., Glen, S. L. W., Livesay, A., Li, G., & Fu, F. H. (2004). In situ forces in the anterior cruciate ligament and its bundles in response to anterior tibial loads. *Journal of Orthopaedic Research*, 15(2), 285–293. https://doi.org/10.1002/jor.1100150219

Shimokochi, Y., & Shultz, S. J. (2008). Mechanisms of noncontact anterior cruciate ligament injury. *Journal of Athletic Training*, 43, 396–408. https://doi.org/10.4085/1062-6050-43.4.396

Shin, C. S., Chaudhari, A. M., & Andriacchi, T. P. (2011). Valgus plus internal rotation moments increase anterior cruciate ligament strain more than either alone. *Medicine & Science in Sports & Exercise*, 43(8), 1484–1491. https://doi.org/10.1249/MSS.0b013e31820f8395

Sigward, S. M., & Powers, C. M. (2006). The influence of gender on knee kinematics, kinetics and muscle activation patterns during side-step cutting. *Clinical Biomechanics*, 21, 41–48. https://doi.org/10.1016/j.clinbiomech.2005.08.001

Sigward, S. M., & Powers, C. M. (2007). Loading characteristics of females exhibiting excessive valgus moments during cutting. *Clinical Biomechanics*, 22(7), 827–833. https://doi.org/10.1016/j.clinbiomech.2007.04.003

Solomonow, M., Baratta, R., Zhou, B. H., Shoji, H., Bose, W., Beck, C., and D'ambrosia, R. (1987). The synergistic action of the anterior cruciate ligament and thigh muscles in maintaining joint stability. *American Journal of Sports Medicine*, 15(3), 207–213. https://doi.org/10.1177/036354658701500302

Vanrenterghem, J., Venables, E., Pataky, T., & Robinson, M. A. (2012). The effect of running speed on knee mechanical loading in females during side cutting. *Journal of Biomechanics*, 45(14), 2444–2449. https://doi.org/10.1016/j.jbiomech.2012.06.029

von, P. A., Roos, E. M., & Roos, H. (2004). High prevalence of osteoarthritis 14 years after an anterior cruciate ligament tear in male soccer players: A study of radiographic and patient relevant outcomes. *Annals of the Rheumatic Diseases*, 63(3), 269. https://doi.org/10.1136/ard.2003.008136

Wannop, J. W., Worobets, J. T., & Stefanyshyn, D. J. (2010). Footwear Traction and Lower Extremity Joint Loading. *American Journal of Sports Medicine*, 38, 1221–1228. https://doi.org/10.1177/0363546509359065

Welinski, M. L., Lee, L. N., McBroom, B., Mufarreh, B., & Gidley, A. D. (2021). Ground reaction forces and temporal characteristics define cutting performance. *International Journal of Exercise Science*, 14(1), 211–221. https://digitalcommons.wku.edu/ijes/vol14/iss1/5/

Winter, D. A. (2005). *Biomechanics and motor control of human movement third edition*. John Wiley & Sons, Inc.